Applied Occupational and Environmental Hygiene

ISSN: 1047-322X (Print) 1521-0898 (Online) Journal homepage: https://www.tandfonline.com/loi/uaoh20

# Comparison of Mathematical Models for Exposure Assessment With Computational Fluid Dynamic Simulation

James S. Bennett , Charles E. Feigley , Jamil Khan & Mohamed H. Hosni

**To cite this article:** James S. Bennett , Charles E. Feigley , Jamil Khan & Mohamed H. Hosni (2000) Comparison of Mathematical Models for Exposure Assessment With Computational Fluid Dynamic Simulation, Applied Occupational and Environmental Hygiene, 15:1, 131-144, DOI: 10.1080/104732200301953

**To link to this article:** https://doi.org/10.1080/104732200301953

Published online: 30 Nov 2010.

Submit your article to this journal

Article views: 82

View related articles

Citing articles: 10 View citing articles

Full Terms & Conditions of access and use can be found at
https://www.tandfonline.com/action/journalInformation?journalCode=uoeh20

Applied Occupational and Environmental Hygiene
Volume 15(1): 131–144, 2000
Copyright © 2000 Applied Industrial Hygiene
1047-322X/00 $12.00 + .00

# Comparison of Mathematical Models for Exposure Assessment With Computational Fluid Dynamic Simulation

**James S. Bennett,[1,] *Charles E. Feigley,[1] Jamil Khan,[2] and Mohamed H. Hosni[3]**
[1]*Department of Environmental Health Sciences, University of South Carolina, Columbia, South Carolina;*
[2]*Department of Mechanial Engineering, University of South Carolina, Columbia, South Carolina;*
[3]*Institute for Environmental Research, Kansas State University, Manhattan, Kansas*

**For many years exposure to airborne contaminants has been estimated by air or biological monitoring. In occupational settings, mathematical models increasingly are employed as adjuncts to monitoring, for instance, during process design or in retrospective epidemiological studies. Models can make predictions in a wide variety of scenarios, can be used for rapid screening, and may reduce the need for monitoring in exposure assessment. However, models make simplifying assumptions regarding air flow and contaminant transport. The errors resulting from these assumptions have not been systematically evaluated. Here we compare exposure estimates from the single-zone completely mixed (CM-1), two-zone completely mixed (CM-2), and uniform diffusivity (UD) models with workroom concentration fields predicted by computational fluid dynamics (CFD). The room air flow, concentration fields, and the breathing zone concentration of a stationary worker were computed using Fluent V4.3 for factorial combinations of three source locations, three dilution air flow rates and two emission rate profiles, constant and time-varying. These numerical experiments were used to generate plausible concentration fields, not to simulate exactly the processes in a real workroom. Thus, "error" is defined here as difference between model and CFD predictions. For both constant and time-varying emission sources, exposure estimates depended on receptor and source location. For the constant source case, ventilation rate was shown to be inconsequential to CM-1 model error. CM-1, CM-2, and UD models differed in their agreement with CFD. UD was closest to CFD for estimating concentration in the simulated breathing zone (BZ) near the source, although large errors resulted when the model was applied to the plane of possible breathing zones. CM-1 performed better for this plane but underestimated the near-source BZ exposure. For the near-source BZ location, CM-2 replicated CFD predictions more closely than CM-1 did, but less closely than UD did. Error in CM-1 model estimation of short-term average exposure to a time-varying source was highly dependent on ventilation rate. Error decreased as ventilation rate increased.**

**Keywords** CFD, Source Location, Monitoring Location, Mathematical Models, Mass Balance, Eddy Diffusivity, Mixing, Residence Time, Ventilation

Contaminant concentration in occupational environments is a function of position and time. This behavior can be expressed as a concentration field, $C(x, y, z, t)$. Workplace air monitoring generally measures only a small portion of this field. Exposure assessments often require more complete concentration information than typical monitoring data provide. Examples are the reconstruction of historical exposures and determining probability of exceeding an exposure limit anywhere in a work area based on monitoring at specific locations. The lack of complete information regarding the concentration field leads to the use of models that rely on simplifying assumptions, for instance, assuming the concentration in a room is uniform. However, the concentration in typical workrooms with sources and air exchange is not uniform. Note that in this article, exposure refers to concentration available for respiration, without consideration of transport and absorption in vivo.

Keil et al.[(1)] applied a model, here called the uniform diffusivity (UD) model, that assumes a contaminant is transported from the source by isotropic turbulence. They obtained eddy

*Current address: National Institute for Occupational Safety and Health, Division of Physical Sciences and Engineering, Engineering Control Technology Branch, 4676 Columbia Parkway, R5, Cincinnati, OH 45226.

diffusivity measurements for use in the hemispherical mass balance equation for isotropic diffusion,

$$C = \frac{G}{2\pi \mathrm{rD}}\left[1 - \mathrm{erf}\left(\frac{r}{\sqrt{4Dt}}\right)\right]. \quad [1]$$

The steady-state form is,

$$C = \frac{G}{2\pi rD}. \quad [2]$$

The diffusivity measurements were made by releasing a tracer gas at a known rate, $G$, measuring the concentration, $C$, at a certain distance, $r$, from the source, and solving for $D$. A refinement of the UD model is the incorporation of "cross-drafts".[2] Here the air speed and direction must be known. However, the air velocity vector may not be measurable in most indoor occupational environments. In outdoor work settings near equipment or buildings, the ambient velocity field may be highly complex.

Shade and Jayjock carried out a Monte Carlo analysis using the UD concept.[3] Exposure during indoor and outdoor bromination was modeled. For the indoor case a range of diffusivities, 0.12–4.2 $m^3$/min, reported by other eddy diffusivity investigators was used. For the outdoor case horizontal diffusivity was calculated using general U.S. wind data and a diffusivity-wind relation which assumed a Pasquill-Guifford Stability Class D (neutral stability).

The other major model used in exposure assessment is the completely mixed (CM) model for dilution ventilation, which has many variations. This model results when the concentration in the contaminant mass balance is assumed to be uniform throughout the room volume, $V$. If the exhaust flow, $Q$, and the contaminant generation rate, $G$, are constant, the time-dependent mass balance may be written as,

$$G = V\frac{dC}{dt} + QC, \quad [3]$$

or in steady-state form as,

$$G = QC.[4] \quad [4]$$

There are several modifications to this model which can make it more accurate, general, or more appropriate. $Q$ can be replaced by an *effective* ventilation rate to account for uneven distribution of dilution air and spatial concentration variability.[4] This technique of using a safety factor or a mixing factor is more frequently used in specifying dilution air flow rates than in exposure estimation. Mage and Ott argued that applying a mixing factor to a single compartment model is flawed because the mass balance principle is violated. For exposure assessment in rooms with concentration gradients, they recommended using multiple zones instead of a mixing factor.[5]

In the two-zone model (CM-2) used by Nicas, mass balances are applied to a zone that includes the contaminant source and to the remainder of the room volume.[6] These zones are termed near-field and far-field, respectively. Equations like 3 and 4 are written for both zones, and the system of two equations is solved to yield the concentrations. Determination of the inter-zone air exchange rate is a difficulty of the method, although it can be found from the mass balance equations if the near-field zone concentration, generation rate, and ventilation rate are known. Another issue is the size, location, and geometry of the zones. Complete mixing is assumed within each zone, which for the near-field is especially problematic given the large concentration gradient commonly found there.

Although the CM and UD models are used increasingly in exposure assessment, they have not been systematically evaluated. The goal here is to demonstrate the impact of dilution air flow rate and source location on model performance for constant rate and time-varying sources in a workroom. The investigation of these models requires a more accurate standard for comparison, such as a comprehensive field study, a full-scale experiment, a scale model experiment, or numerical simulation.[7] Experimental approaches require measurement of $C$ throughout the space, or at least at many important locations. This can be very time-consuming and expensive, especially so in a full-sized room. Real workrooms are not ideal for parametric studies because many important factors cannot be varied. Full-scale experimental simulations can be designed for control of some of these factors, but at great cost. Scale models can closely replicate the significant characteristics of real rooms at less expense, but all scaling criteria cannot be satisfied simultaneously.[8] Numerical simulation, called computational fluid dynamics (CFD), has the advantages of costing less, consuming less time, allowing easy manipulation of parameters, and providing complete information on concentration and other important variables throughout the room. Also, CFD solutions are free of sampling and analytical errors, and scaling compromises. Like other analytical approaches, however, CFD involves some degree of idealization of conditions. Boundary conditions may be difficult to specify accurately, and turbulence is modeled, at least in part. Thus, we have used CFD to explore the effects of air flow rate and source location on model error, recognizing that CFD is an approximation.

The workroom described by Stewart et al.[9] for studying embalmer's exposures was used as a prototype for these investigations. No attempt was made to exactly simulate the air flow and contaminant dispersion in this room. Instead, the setting provided a plausible scenario for examining the effects of the variables of interest. Indeed exact simulation of this room is not possible because the thermal boundary conditions are not known, the movements of three people working in the room were not recorded, and the locations of many of the sources are not known accurately (such as fluid spill on the floor).

## METHODS

### CFD Methods

The numerical simulations were performed using the commercial CFD software, Fluent, applying the control volume method and the SIMPLE algorithm described by Patankar.[10] The $k$-$\varepsilon$ turbulence model put forth by Spalding was utilized.[11] Because 3-D time-dependent concentration fields were simulated, the $k$-$\varepsilon$ turbulence model was chosen for economy, because

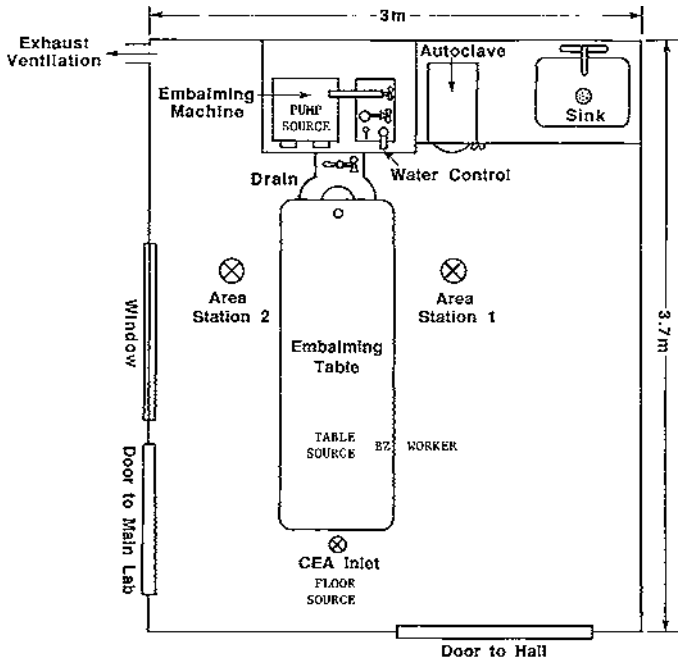


**FIGURE 1**
Room layout showing source and receptor locations.

it requires less computational effort than more sophisticated models. The room simulation was constructed using a uniform grid of 10,400 rectangular cells, 16.6 × 17.1 × 15.4 cm. Objects within the room and the worker were also built from these rectangular cells.

Figure 1 is a plan view of the actual room, showing monitoring and source locations. The "monitoring" locations in the simulation correspond to those in Stewart et al., except that the breathing zone (and "worker") was stationary and the exhaust concentration was also monitored. The breathing zone exposure was monitored in the simulation by finding the concentration at the center of the cell directly in front of the worker's face. The height of this location was 1.46 meters. This height was very close to the average height of the breathing zones of the 50th percentile man and woman, 1.5 meters, if the breathing zone height is assumed to be midway between the mouth and nose.[12] Three source locations representative of those observed in Stewart et al. were used for these simulations.[9] The room consisted of a pedestal-mounted embalming table with a urinal-type drain, equipment on a countertop, shelves, cabinets, a 61-cm (standard two-foot) square ceiling mounted supply air diffuser, and an approximately 15-cm-square exhaust outlet next to a room corner and near the floor. "Live" cells composed the room interior where the concentration field was determined. "Wall" cells were used at solid boundaries and to build objects. "Inlet" cells were used for ventilation supply air and for air contaminant source emission. To produce $Q$, the normal velocity through the supply air cell faces was specified, given the known cell face area. Tangential velocity components obtained by experimental measurements of the supply air diffuser were also specified. To produce $G$, the contaminant mole fraction and velocity normal to the source inlet cell faces were specified, resulting in volume of contaminant per unit time. Figure 2 shows the representation of the room in CFD. The black square indicates the table source

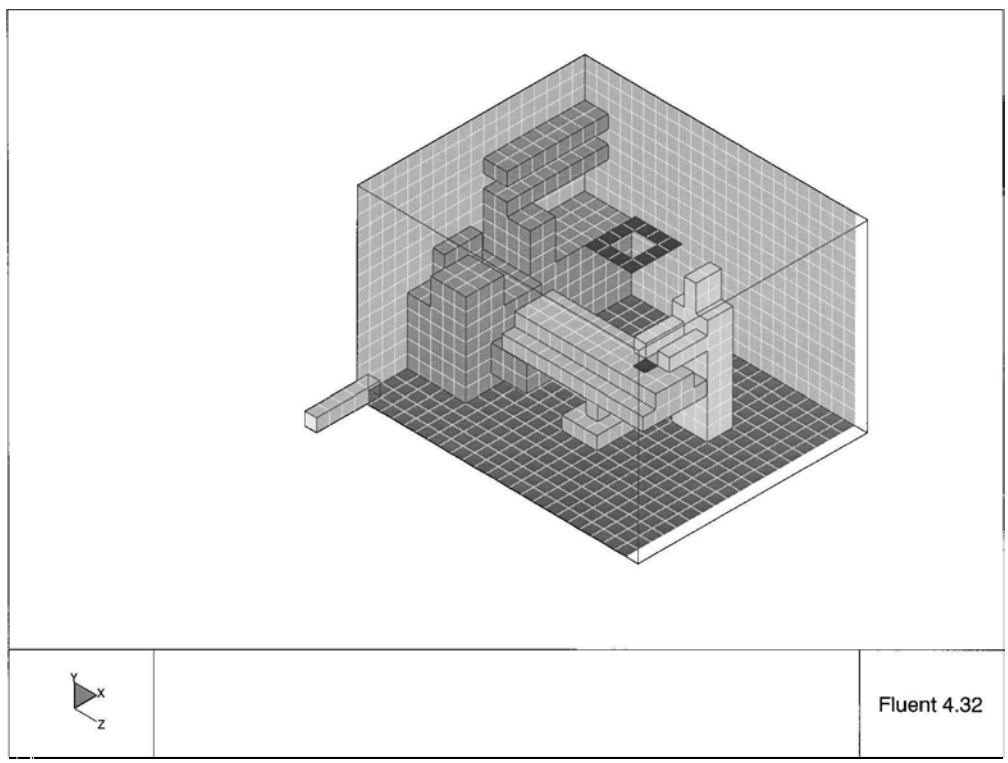


**FIGURE 2**
Room representation in CFD simulation.

location. The floor and pump source locations are shown in subsequent figures. The solution was considered converged if the sum of the normalized residuals for each conservation equation was less than $10^{-5}$.

The final solutions were validated using grid and time step independence, physical plausibility, and experimental data in the literature. The time-dependent simulations do not require separate validation via grid independence because each time step is itself a kind of steady-state solution. For time-dependent cases the high ventilation rate and pump source were chosen for validation tests because this combination proved to be the most challanging to simulate. As a measure of physical plausibility for the steady-state case, the exhaust concentration was compared to $G/Q$. In the time-dependent case, the emission estimate taken in the exhaust was compared with the time integral of $G$. To externally validate the simulations experimental results for a similar room used in another study, a full-sized test room described by Hosni et al., were compared with numerical simulations for that room, using CFD methods identical to the present study.[13]

Returning to the present study, the flow out of the ceiling diffuser was simulated as accurately as possible, because preliminary investigation had determined that this flow had a crucial influence on the flow in the room as a whole. Zhang et al. also reported this influence.[14] To that end, the supply portion of the ventilation system was reproduced in the laboratory. Velocity measurements at the diffuser were used as boundary conditions in the simulation, like the methods developed by Nielsen.[15,16] A fan drove flow through the same diameter and type of flexible duct and out of the same type and size of ceiling diffuser. Importantly, the lengths and angles of the ductwork were reproduced, so that the loading of one side of the diffuser was replicated. Turbulence quantities were also specified. The turbulence intensity was taken as 10 percent, which is common practice, when this quantity is not measured. The turbulence length scale was set at 3.81 cm, the separation between vanes of the diffuser, using the idea that an eddy can be no larger than the flow boundary allows.[17] Turbulent flows created by worker motion were not included in the simulation. The simulations were performed under isothermal conditions.

The room interior and the worker were "constructed" in the simulation using measurements and photographs of the actual (physical) room. However, the size and shape of the human body and the various and sundry objects found in an occupational setting can only be approximated, when built from the uniform rectangular solids that reduced the required computational time. Fortunately, smaller objects that cannot be rendered as faithfully effect the flow field less than larger objects that can be represented more accurately. Moreover, an exact simulation of this room was not the goal.

For the steady-state case a nominal contaminant generation rate was arbitrarily chosen, because the absolute concentration levels in the room were not at issue. Instead, the relative variation in the concentration field $C(x, y, z, t)$ drove the investigation. In the time-dependent case, an estimated generation rate function from earlier work was adopted.[18] This generation rate function, shown in Figure 3, corresponded to a work

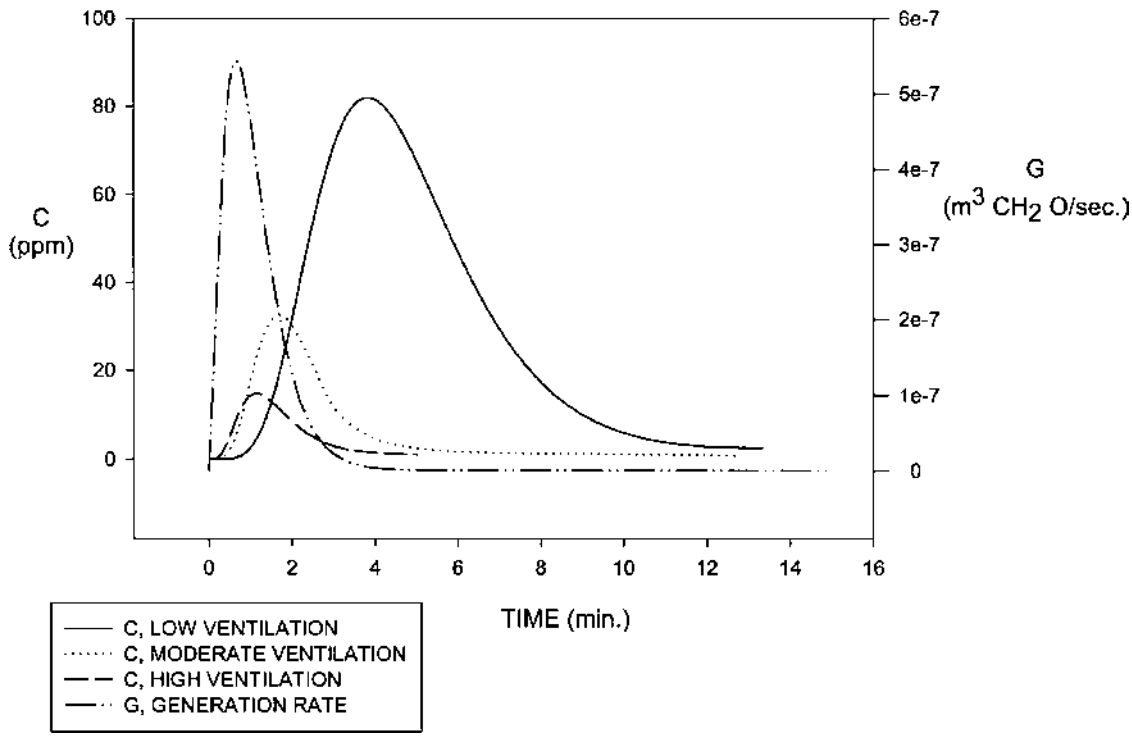


**FIGURE 3**
Concentration and generation rate versus time.

task that contributes highly to formaldehyde exposure during embalming, the application of osmotic gel. It had the steepest rise and fall of the important generation rate functions reported in Bennett et al.[18] As with the steady-state rate, the selection of the time-dependent rate function was somewhat arbitrary and only serves to illustrate the effect of factors on model prediction. Three source locations were chosen for the placement of contaminant inlet cells based on observations made during Stewart's study.[9]

### Experimental Design

Once $C(x, y, z, t)$ was obtained through CFD simulation, complete exposure information was available for thousands of locations in the room volume. Particular attention was paid to the four monitoring locations where data was collected in the study conducted by Stewart et al.[9] Also, the concentration in the exhaust duct was followed closely. These five locations will be referred to as the receptor locations. In evaluating the CM-1 model for the constant source case, the steady-state concentrations at the five receptor locations were compared. For the CM-1 and UD models the difference in concentration between the model prediction and the CFD simulation was calculated for the entire plane at the height of a typical standing breathing zone. The steady-state concentration represented a time-weighted average (TWA) for any period of interest. For the time-dependent case, the short-term (15-minute) average was the basis of comparing the simulation results to the model predictions.

Table I summarizes the experimental design. These comparisons were done at three ventilation rates to investigate the effects of this variable on the accuracy of exposure estimates. Additional flow rates were utilized to establish an empirical relationship between ventilation rate and concentration. These additional simulations were carried-out for the special case of a constant source on the table and the BZ receptor location, the most critical exposure scenario.

### Calculation of Model Estimates

The CM-1 steady-state concentration estimates were found by solving Equation 4 for $C$, given the $G$ and $Q$ values used as boundary conditions in the simulations. For the CM-2 model, the near field was constructed as a hemisphere with radius equal to the distance between the center of the source cell and the center of the BZ cell.[6] The average air speed upwind of the worker was multiplied by the projected area of the hemisphere to approximate the inter-zone exchange rate, $\beta$. The completely mixed near field concentration was then:

$$C_{NF} = \frac{G}{Q} + \frac{G}{\beta}. \quad [5]$$

$C_{NF}$ was compared to $C_{BZ}$. To apply the UD model, the eddy diffusivity, $D$, was calculated from Equation 2 using the concentrations at A1, A2, BZ, and CEA, resulting from the three source locations. Thus, $D$ was calculated along 12 distinct paths in the room. The average of these values was interpreted as the isotropic eddy diffusivity for the room. This calculation was repeated at each ventilation rate.

For the time-dependent case, Equation 3 was solved numerically for $C$, the instantaneous concentration predicted by the CM-1 model. A 15-minute average was applied to this function and compared to the 15-minute averages for the concentration functions at the monitoring locations, $C_{A1}(t)$, $C_{A2}(t)$, $C_{BZ}(t)$, $C_{CEA}(t)$, and $C_{EX}(t)$.

## RESULTS AND DISCUSSION

### CFD Validation

The results from the original grid were compared to a new grid where the number of cells in the room volume is doubled in each direction (the number of cells in the room volume increases by a factor of eight). Cell dimensions of the new grid were $8.28 \times 8.59 \times 7.72$ cm. The absolute value of the percent difference between steady-state concentrations over all combinations of source location, receptor location, and ventilation rate had a median value of 4.24 percent. The median was used because a small number of large differences skewed the distribution. The differences ranged from $-58.0$ percent to 25.0 percent. Given that accuracy of the $k$-$\varepsilon$ turbulence model has some limitations for simulating room flows[19] and that room objects and the human body were approximated with a uniform rectangular grid, the economy of the original grid solution is a sound trade-off to the precision of the finer grid solution. Thus, for flows in this simulation that are near objects and/or effected by turbulence, it is not clear that the finer grid will be a more realistic solution, particularly when the original grid satisfies all applicable conservation laws. For these reasons the original grid solution was used.

**TABLE I**
Experimental design

| | CM-1 | CM-2 | UD |
|---|---|---|---|
| Source location | Floor, pump, table | Floor, pump, table | Floor, pump, table |
| Source type | Constant<br>Time-varying | Constant | Constant |
| Receptor location | A1, A2, BZ, CEA, EX<br>BZ height plane | BZ | BZ<br>BZ height plane |
| Ventilation rate ($m^3$/min) | 0.522, 2.44, 6.23 | 0.522, 2.44, 6.23 | 0.522, 2.44, 6.23 |

The concentration as a function of time at the five receptor locations for both the original time step of 0.5 seconds and the reduced time step, 0.25 seconds were compared and found to be indistinguishable. This showed that the numerical solution was not improved by a shorter time step. As explained above, the results for the high ventilation rate and the pump source represent the worst case.

As external validation Figure 4 shows the percent difference between experimental measurements and numerical simulation of air speed for a room with many of the same characteristics.[13,20] That simulation used a coarser grid than the present study. The data are for the room centerplane, parallel to the main flow direction. The flow is symmetric about this plane. The Y-coordinate is the distance below the ceiling. The line indicating standing breathing zone height is 1.5 meters above the floor. This contour plot indicates that the difference is less than 30 percent in all areas where a source or receptor might be located. Also, the difference is negligible for a large portion of the plane. The room Reynolds number is 2400. Although this is higher than the range of values for the present study, 173–2066, these correspond to an open room, whereas objects in a room create more turbulence.

Air velocity measurements were made simultaneously with both an omni-directional and a three-dimensional hot-film probe. Due to both magnitude (<0.15 m/s) and direction (within a 70 degree cone angle) limitations of the three-dimensional probe, only the mean air velocity from this probe in locations where the airspeed was greater than 1.0 m/s was used. The omni-directional probes are best-suited for low air speed measurements in flow fields where the flow direction is unknown or is difficult to evaluate. Thus, a 0–1.0 m/s range omni-directional probe was used to measure the airspeed outside the jet region and in locations where the airspeeds were less than 1.0 m/s.

The airspeed was used for validation of CFD predictions instead of velocity components measured by the three-dimensional probe because outside the jet region, the measured velocity components were not reliable due to the uncertainty in determination of the flow direction and the lower velocity limit of the probe. Furthermore, in the jet region, the axial velocity component has approximately the same magnitude as the airspeed. Thus, airspeed was a logical choice for validation because the jet core direction is known and the jet plays a major role in the general room air flow distribution. Measured air speeds in the occupied region (from floor to 1.8 m high) were found to be typical of indoor work environments. In a recent survey of 55 workplaces, approximately 85 percent of the measurements were below 60 ft/min (0.30 m/s),[21] indicating the difficulty of experimental determination of indoor velocity fields.

## Exposure Estimation for Constant Source

The simulated steady-state concentrations for a constant source and moderate ventilation rate are shown in Table II for the combinations of five receptor or "monitoring" locations and three source locations. Breathing zone concentration varies from the values for other locations and the CM-1 model estimate, 6.69 ppm. By definition, in real rooms the steady-state exhaust concentration is equal to the CM concentration. The CFD concentration found for the exhaust duct is in accord with this fact. Defined here as difference between CFD and model predictions, the "error" in the CM-1 model ranged from −73.7 percent to + 54.8 percent. The extremes occurred for the BZ location. Interestingly, the error ranged from −73.7 percent to + 96.3 percent,

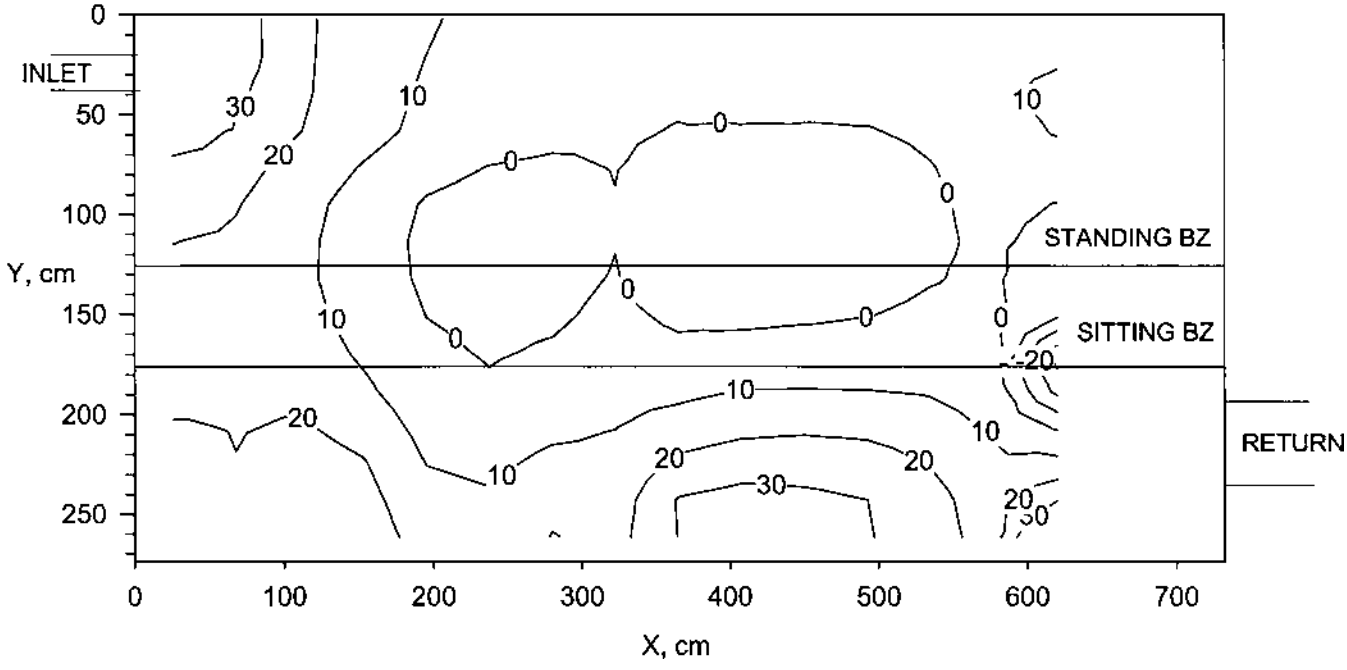


**FIGURE 4**
Simulated and experimental airspeed percent difference.

**TABLE II**
Steady-state concentration and CM-1 error for moderate ventilation rate

| | CM-1 (ppm) | Area 1 (ppm/%) | Area 2 (ppm/%) | Breathing zone (ppm/%) | CEA (ppm/%) | Exhaust (ppm/%) |
|---|---|---|---|---|---|---|
| Floor source | 6.69 | 6.79/−1.49 | 8.48/−21.1 | 4.32/54.8 | 4.66/43.5 | 6.69/0.00 |
| Pump source | 6.69 | 9.43/−29.1 | 6.34/5.50 | 6.39/4.67 | 6.08/10.0 | 6.69/0.00 |
| Table source | 6.69 | 6.68/0.13 | 8.11/−17.5 | 25.4/−73.7 | 14.2/−52.9 | 6.69/0.00 |

if the concentration at the other monitoring locations is taken to represent the BZ concentration, holding source location constant. Thus, the BZ concentration was somewhat better represented by the complete mixing assumption than by area monitoring. This makes sense considering that the CM concentration was bracketed by the values at specific locations, thus moderating the strong effect of receptor location. However, it remains that in this simulated workroom both area monitoring and estimates using the well-mixed mass balance relation poorly represented personal exposure.

The simulated concentration fields at breathing zone height are shown graphically in Figures 5–7, for the floor, pump, and

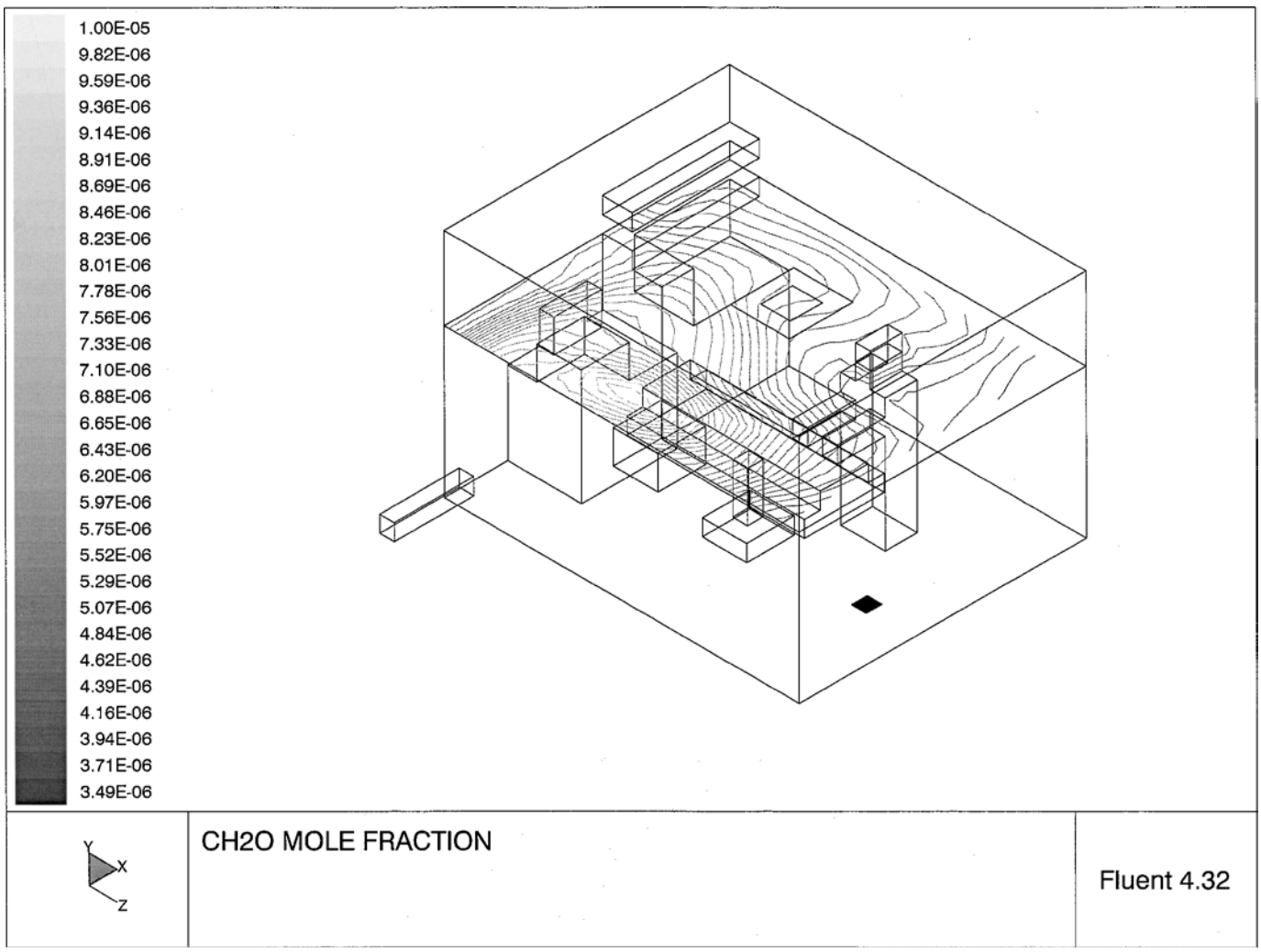


**FIGURE 5**
Concentration contours at breathing zone height, source on floor.

table source locations, respectively, at the moderate ventilation rate. In this isometric view of the room, contours of constant concentration are plotted for a horizontal plane 1.5 meters above the floor. The lighter shades of gray indicate the higher concentrations. The contaminant source is the black square. These graphs show the range of concentration and the complexity of the pattern. Note that only for the table source was the highest breathing zone plane concentration directly above the source. For the floor source the maximum was closer to the exhaust than the source. Thus, the conventional idea that concentration is everywhere decreasing with distance from source is shown not to apply. It is tempting to then conclude that the region of maximum concentration was drawn toward the exhaust, as with local exhaust ventilation. However, this did not occur for the pump source. The maximum was between the worker and the source, and not between the source and the exhaust. The value of CFD in computing the concentration field is apparent when intuition fails.

Having seen how the concentration fields vary with location, it is natural to think about the mass transport processes in room air. To the results shown earlier, the factor of ventilation rate is incorporated. Figure 8 shows the velocity vectors at breathing zone height for the moderate ventilation rate. The same pattern was observed for low and high ventilation.

Figures 9 and 10 show that simulated concentration at a specific location was linearly related to $(G/Q)$. This was true for each source location, although it is shown here for the table source. Regression analysis gives an $R^2$ greater than 0.998 for each line. In other words, the error in the CM-1 model is nearly constant across ventilation rate. This relation is useful because if concentration at a location of interest, $C_i$, is known at a certain ventilation rate, $Q_1$, the concentration at another ventilation rate can be found from the ratio:

$$\frac{C_{i2}}{C_{i1}} = \frac{G/Q_2}{G/Q_1} = \frac{Q_1}{Q_2}. \qquad [6]$$

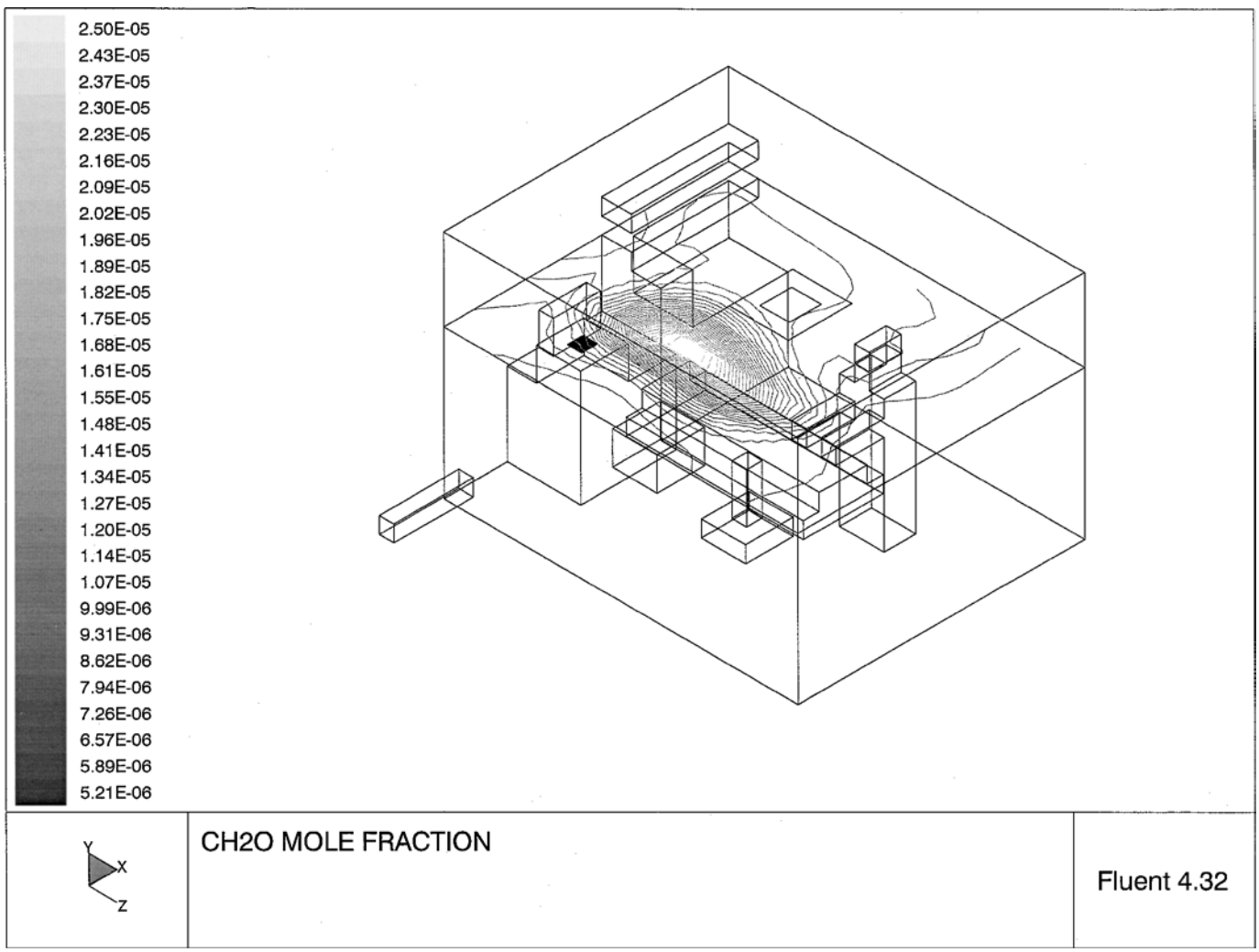


**FIGURE 6**
Concentration contours at breathing zone height, source at pump.

The location-specific error in the CM-1 model is conveniently defined as a *location factor*, $\lambda_i$, where:

$$\lambda_i = \frac{C_i}{(G/Q)}. \quad [7]$$

The $\lambda_i$ are the slopes of the lines in Figures 9 and 10.

Table III compares the BZ concentration for the table source using CFD and the CM-1, CM-2, and UD models. The UD model has represented the simulated BZ concentration more accurately than the CM models. Generalizing the BZ location to include the room plane at breathing zone height, the CM-1 model is tighter than the UD model around the simulated values, as shown by the error ranges of −88 percent to +26 percent for CM-1, and −67 percent to +192 percent for UD. The CM-2 model was not evaluated for the plane because its near field is defined in relation to both the source and the worker.

**TABLE III**
Comparison of models (BZ concentration in ppm/percent error)

| $Q$ ($m^3$/min) | CFD | CM-1 | CM-2 | UD |
|---|---|---|---|---|
| 0.522 | 145.00 | 31.26/−78.44 | 77.44/−46.59 | 95.10/−34.42 |
| 2.44 | 25.40 | 6.69/−73.67 | 15.67/−38.33 | 20.89/−17.75 |
| 6.23 | 9.97 | 2.62/−73.73 | 6.04/−39.45 | 8.21/−17.68 |

### Exposure Estimation for Time-Varying Source

For the time-dependent source at the table, the instantaneous concentrations at the four monitoring locations and the exhaust duct are shown in Figures 11 through 13 for some of the simulations. Here, the exhaust concentration is more interesting than in the steady-state case because of the delay in contaminant

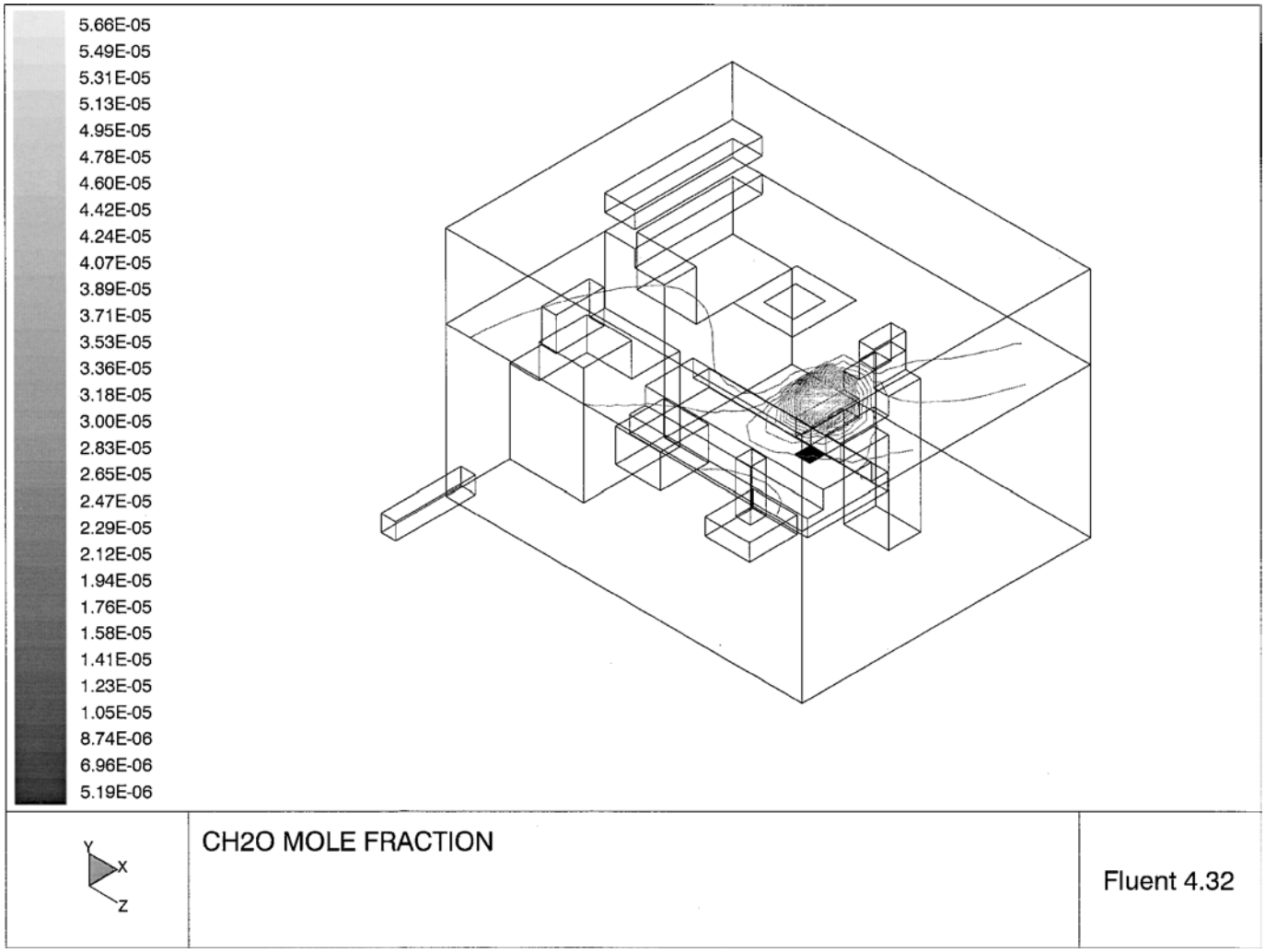


**FIGURE 7**
Concentration contours at breathing zone height, source at table.

**TABLE IV**
15-minute average concentration for moderate ventilation rate

| | Area 1 (ppm) | Area 2 (ppm) | BZ (ppm) | CEA (ppm) | Exhaust (ppm) | Average (ppm) |
|---|---|---|---|---|---|---|
| Floor | 1.03 | 1.43 | 0.543 | 0.636 | 1.03 | 0.934 |
| Pump | 1.44 | 0.901 | 0.834 | 0.810 | 0.949 | 0.987 |
| Table | 0.884 | 1.19 | 5.12 | 2.36 | 0.909 | 2.09 |
| Average | 1.12 | 1.17 | 2.17 | 1.27 | 0.963 | 1.34 |

reaching the exhaust. Of particular interest to industrial hygienists is the short-term average concentration. The 15-minute average concentrations are shown in Table IV for the combinations of five receptor and three source locations. It can be seen that both the source location and the receptor location had an impact on the instantaneous and time-averaged concentrations.

Table V displays how variability in the 15-minute average of the simulated concentration depends on ventilation rate. The last column indicates that the error if CM is assumed, averaged over all locations, decreases as flow rate increases. As Figures 11 through 13 show, the length of time that the room is poorly mixed decreases as flow rate increases. It is apparent that this poorly mixed period causes the error in the CM 15-minute average concentration. Once the concentration has become uniform in the room, $C(t)$ decays exponentially, vis.,

$$C(t - t_0) = C(t_0) \exp\left[-\frac{Q}{V}(t - t_0)\right]. \qquad [8]$$

There is a similarity in shape of these plots across ventilation rate. In other words, source and receptor location are the powerful determinants of the shape of the $C(t)$ function. However, the width of the peaks and the length of the poorly mixed period

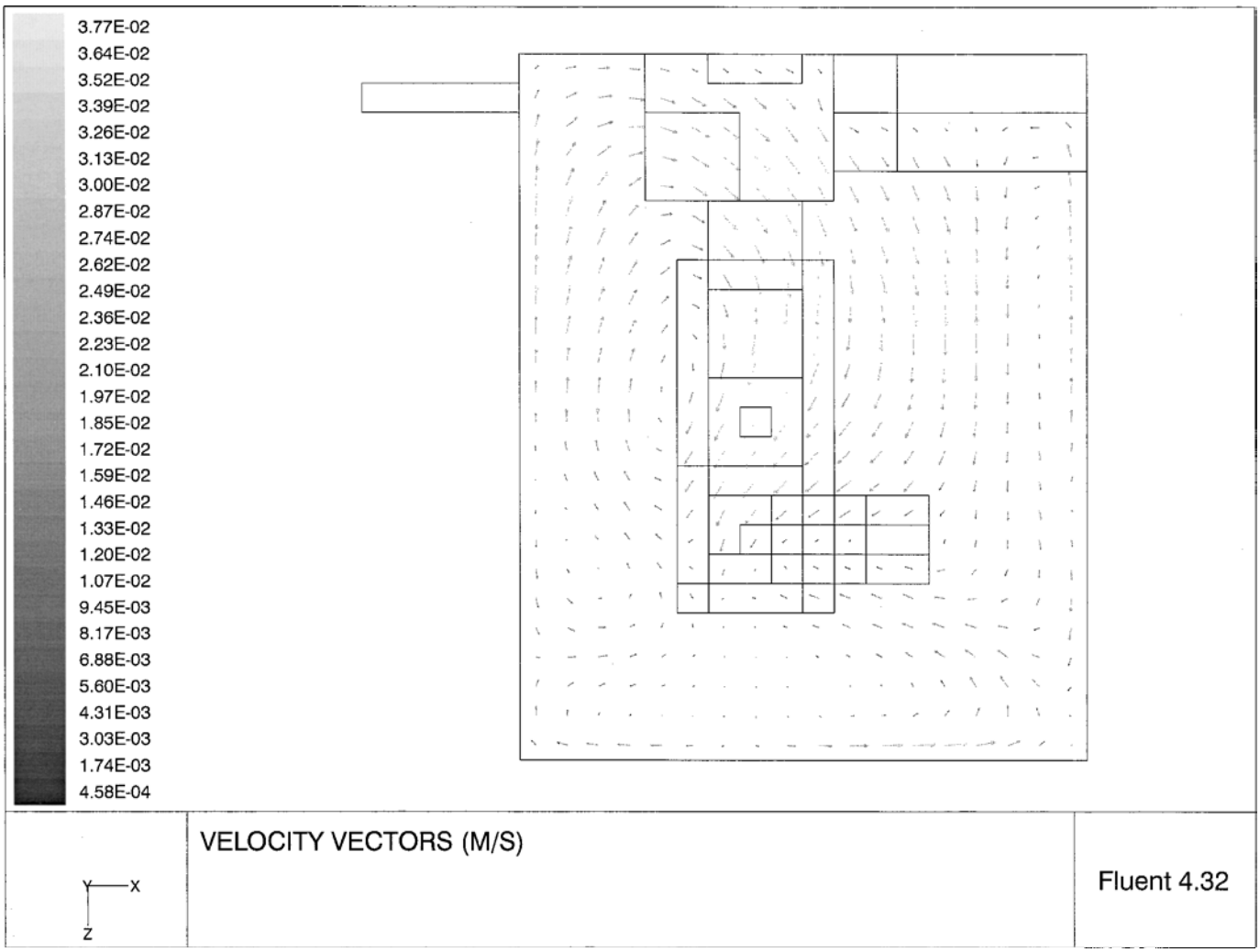


**FIGURE 8**
Velocity vectors at breathing zone height.

**TABLE V**
15-minute average concentration, time-dependent source

| Flow rate ($m^3$/min) | Receptor location | Source location | Concentration (ppm) | CM concentration (ppm) | Error (%) | Mean error absolute value (%) |
|---|---|---|---|---|---|---|
| 0.522 | A1 | Floor | 0.72 | 1.50 | 107.18 | 312.24 |
| | | Pump | 2.94 | 1.50 | −48.98 | |
| | | Table | 0.18 | 1.50 | 737.99 | |
| | A2 | Floor | 4.31 | 1.50 | −65.20 | |
| | | Pump | 1.10 | 1.50 | 36.36 | |
| | | Table | 0.67 | 1.50 | 122.55 | |
| | BZ | Floor | 0.08 | 1.50 | 1820.61 | |
| | | Pump | 0.20 | 1.50 | 642.57 | |
| | | Table | 25.10 | 1.50 | −94.02 | |
| | CEA | Floor | 0.86 | 1.50 | 75.23 | |
| | | Pump | 0.38 | 1.50 | 297.88 | |
| | | Table | 7.04 | 1.50 | −78.69 | |
| | EX | Floor | 2.21 | 1.50 | −32.13 | |
| | | Pump | 0.80 | 1.50 | 86.57 | |
| | | Table | 0.28 | 1.50 | 437.63 | |
| 2.44 | A1 | Floor | 1.03 | 0.93 | −9.61 | 27.40 |
| | | Pump | 1.44 | 0.93 | −35.35 | |
| | | Table | 0.88 | 0.93 | 5.32 | |
| | A2 | Floor | 1.43 | 0.93 | −34.90 | |
| | | Pump | 0.90 | 0.93 | 3.33 | |
| | | Table | 1.19 | 0.93 | −21.76 | |
| | BZ | Floor | 0.54 | 0.93 | 71.45 | |
| | | Pump | 0.83 | 0.93 | 11.63 | |
| | | Table | 5.12 | 0.93 | −81.82 | |
| | CEA | Floor | 0.64 | 0.93 | 46.38 | |
| | | Pump | 0.81 | 0.93 | 14.94 | |
| | | Table | 2.36 | 0.93 | −60.55 | |
| | EX | Floor | 1.03 | 0.93 | −9.61 | |
| | | Pump | 0.95 | 0.93 | −1.90 | |
| | | Table | 0.91 | 0.93 | 2.42 | |
| 6.23 | A1 | Floor | 0.49 | 0.47 | −4.66 | 21.75 |
| | | Pump | 0.66 | 0.47 | −28.09 | |
| | | Table | 0.47 | 0.47 | −0.63 | |
| | A2 | Floor | 0.64 | 0.47 | −26.18 | |
| | | Pump | 0.46 | 0.47 | 2.84 | |
| | | Table | 0.58 | 0.47 | −19.21 | |
| | BZ | Floor | 0.31 | 0.47 | 54.43 | |
| | | Pump | 0.44 | 0.47 | 7.29 | |
| | | Table | 2.01 | 0.47 | −76.57 | |
| | CEA | Floor | 0.33 | 0.47 | 41.02 | |
| | | Pump | 0.43 | 0.47 | 10.82 | |
| | | Table | 0.98 | 0.47 | −51.99 | |
| | EX | Floor | 0.48 | 0.47 | −1.26 | |
| | | Pump | 0.48 | 0.47 | −0.84 | |
| | | Table | 0.47 | 0.47 | −0.42 | |

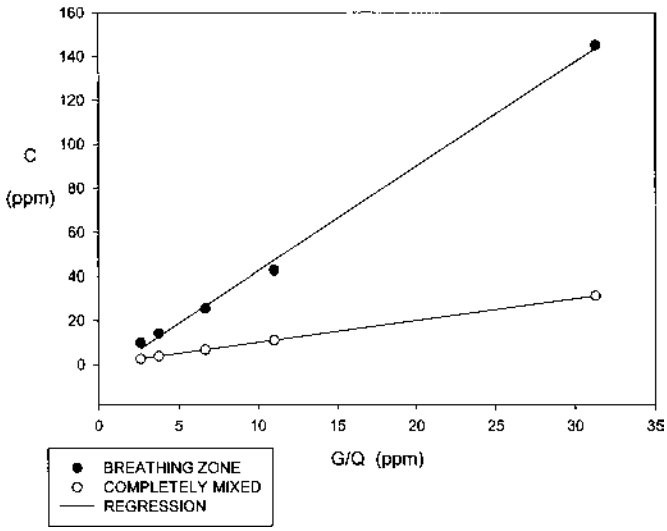


**FIGURE 9**
Breathing zone and completely mixed concentration ($G/Q$) versus $G/Q$.

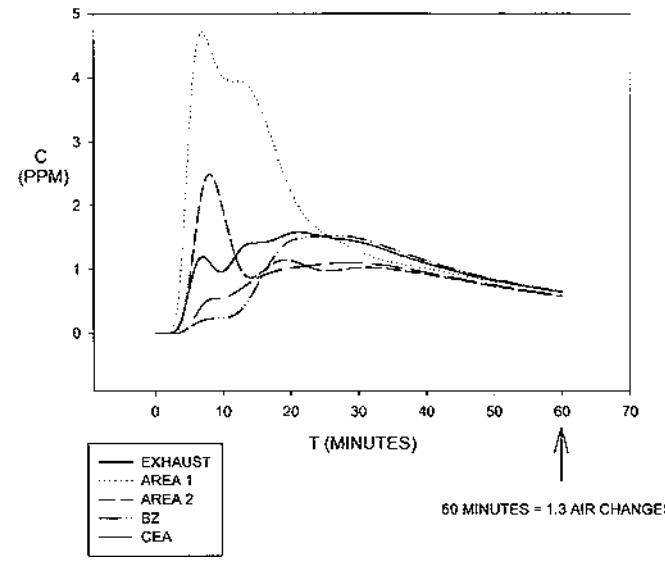


**FIGURE 11**
Concentration versus time, low ventilation, source at pump.

differ in these plots even though the time-axis is scaled according to average residence time. Figure 14 shows this clearly by making time dimensionless. The dimensionless width of the peaks is greatest for the high ventilation rate and least for the low. The low ventilation concentration has decayed to nearly zero after 0.2 air changes, the moderate after 0.6 air changes, and the high after 1.2 air changes. One explanation is that the emission event is *not* scaled accordingly.

Continuing with the table/BZ example, Figure 3 shows the relationship between the emission event and the exposure event under different ventilation rates. The emission event is longer relative to the residence time for the high ventilation situation than for the low. As a consequence, the emission event precedes the low ventilation exposure event, partially coincides with the moderate ventilation exposure event, and completely coincides with the high ventilation exposure event. We now have the tools

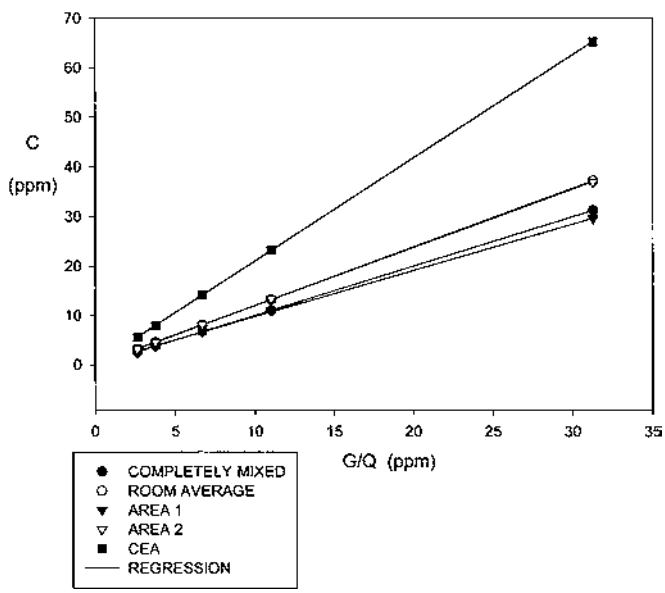


**FIGURE 10**
Concentration at various receptor locations and completely mixed concentration ($G/Q$) versus $G/Q$.

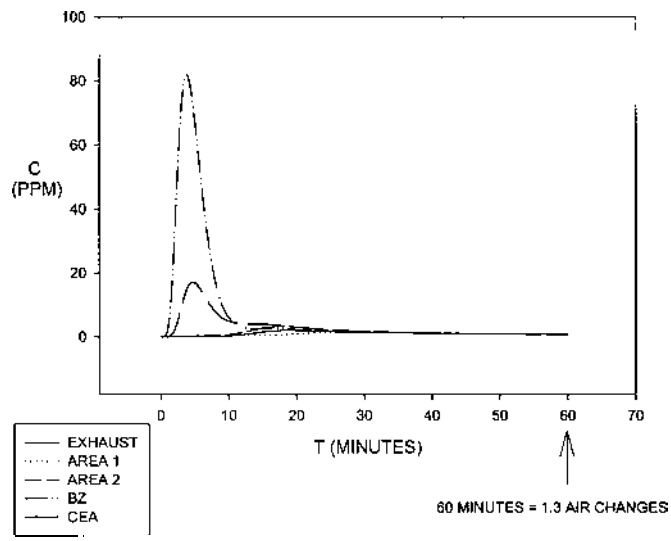


**FIGURE 12**
Concentration versus time, low ventilation, source at table.

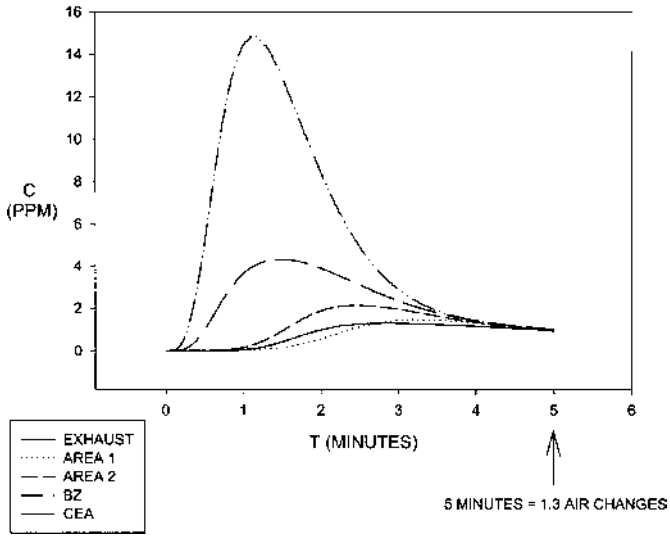


**FIGURE 13**
Concentration versus time, high ventilation, source at table.

to understand why the current study suggests that time-averaged concentration is more spatially uniform for high than for low ventilation, whereas in Bennett et al., there was greatest concentration uniformity at low ventilation.[18] There, time-averaged concentrations at different locations were better correlated for low ventilation than for high.

In the current study the room under high ventilation was well mixed for a greater portion of the 15-minute average than the room under low ventilation. However, in Bennett et al.[18] the correlation was found for full-period averages that were long compared to the time-scale of the emission events. Also, these events were mostly sequential so that emissions occurring early in the embalmings were contributing to the full-period average

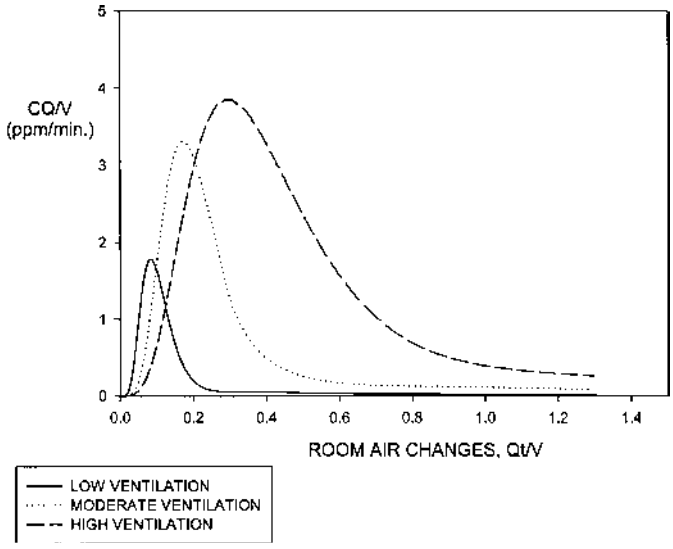


**FIGURE 14**
Normalized concentration versus air changes, source at table, BZ receptor.

in a well-mixed manner for a large portion of the averaging time. This was truest of the low ventilation condition because the residence time was longer.

## CONCLUSION

The results show that, for both constant and time-varying emission sources, exposure estimates depend on receptor and source location. For the constant source case, ventilation rate was shown to be inconsequential to the CM-1 model error. The effect of ventilation rate on exposure was found to be *linear* for the breathing zone and other specific room locations, although the slopes differed. Thus, although spatial variability was a weakness of the CM-1 model, ventilation rate was handled very well. CM-1, CM-2, and UD models differed in their agreement with the CFD results. The concentration estimated using UD was closest to the CFD predictions in the simulated breathing zone near the source, although large errors resulted when the model was applied to the plane of possible breathing zones. CM-1 performed better for this plane overall but underestimated the near-source BZ exposure. For the near-source BZ location, CM-2 replicated CFD predictions more closely than CM-1 did, and less closely than UD did.

The rate of mixing relative to the mean residence time has been demonstrated to be slower for high ventilation rates than for the low, suggesting that, for a time-varying emission source, exposure estimates could depend more strongly on receptor and source location for high ventilation rates than for low. However, this issue has been shown to depend on the averaging interval.

This work provided a strenuous test of the CM model. Also, CFD was found to be a powerful tool for understanding worker exposure and contaminant dispersion. Significantly, it provided a means for evaluating exposure model accuracy, and of conducting numerical experiments to explore the impact of factors such as flow rate, source location, and receptor location on model performance. Relationships were found for a prototype workroom. Research is needed to see how these models perform in other workroom configurations and to confirm, through validation with experimental concentration measurements, the ability of CFD to represent indoor contaminant dispersion patterns.

## REFERENCES

1. Keil, C.; Krupinski, D.; Chamanchkine, M.: Eddy Diffusivity Measurements for Exposure Modeling. In: AIHC&E 1997. Extended Abstract of Paper, American Industrial Hygiene Conference and Exhibition, 182.
2. Keil, C.: In: A Toolbox of Mathematical Models for Occupational Exposure Assessment. Information from Professional Development Course 402, AIHC&E 1996. p. 32.
3. Shade, W.D.; Jayjock, M.A.: Monte Carlo Uncertainty Analysis of a Diffusion Model for the Assessment of Halogen Gas Exposure During Dosing of Brominators. Amer Ind Hyg Assoc J 58:418–424 (1997).
4. American Conference of Governmental Industrial Hygienists (ACGIH): Industrial Ventilation, A Manual of Recommended Practice, pp. 2–2, 2–5. ACGIH, Cincinnati, OH (1988).

5. Mage, T.M.; Ott, W.R.: The Correction for Nonuniform Mixing in Indoor Microenvironments, EPA/600/A-94/196. Environmental Protection Agency (EPA), Washington, D.C. (1994).
6. Nicas, M.: Estimating Exposure Intensity in an Imperfectly Mixed Room. Amer Ind Hyg Assoc J 57:542–550 (1996).
7. Fan, Y.: CFD Modeling of the Air and Contaminant Distribution in Rooms. Energy and Buildings 23:33–39 (1995).
8. Awbi, H.B.: Ventilation of Buildings, pp. 153–158. E & FN SPON, London (1991).
9. Stewart, P.A.; Herrick, R.F.; Feigley, C.E.; et al.: Study Design for Assessing Exposures of Embalmers for a Case-Control Study: Part I. Monitoring Results. Appl Occup Environ Hyg 7:532–540 (1992).
10. Patankar, S.V.: Numerical Heat Transfer and Fluid Flow, pp. 126–131. Hemisphere, New York (1980).
11. Launder, B.E.; Spalding, D.B.: Lectures in Mathematical Models of Turbulence, pp. 74–77, 90–110. Academic Press, London (1972).
12. Tilley, A.R.: The Measure of Man and Woman: Human Factors in Design. Whitney Library of Design, New York (1993).
13. Hosni, M.H.; Tsai, K.; Hawkins, A.N.: Numerical Predictions of Room Air Motion. ASME Fluids Engineering Division Conference Proceedings, vol. 2, (1996).
14. Zhang, J.S.; Christianson, L.L.; Wu, G.J.; et al.: Experimental Evaluation of a Numerical Simulation Model for Predicting Room Air Motion. Ind Environ 2:331–336 (1993).
15. Nielsen, P.V.: The Prescribed Velocity Method—A Practical Procedure for Introduction of an Air Terminal Device in CFD Calculation, ISSN 1395-7953 R9827. Aalborg University, Aalborg, Denmark (August 1998).
16. Nielsen, P.V.: The Box Method—A Practical Procedure for Introduction of an Air Terminal Device in CFD Calculation, ISSN 1395-7953 R9744. Aalborg University, Aalborg, Denmark (December 1997) .
17. Hinze, J.O.: Turbulence, p. 4. McGraw-Hill, New York (1975).
18. Bennett, J.S.; Feigley, C.E.; Underhill, D.W.; et al.: Estimating the Contribution of Individual Work Tasks to Room Concentration: Method Applied to Embalming. Amer Ind Hyg Assoc J 57:599–609 (1996).
19. Emmerich, S.J.: Use of Computational Fluid Dynamics to Analyze Indoor Air Quality Issues, NISTIR 5997, p. 3. National Institute of Standards and Technology (1997).
20. Hawkins, A.N.; Hosni, M.H.; Jones, B.W.: A Comparison of Room Air Motion in a Full Size Test Room Using Different Diffusers and Operating Conditions. ASHRAE Trans, vol. 101, pt. 2. pp. 81–100 (1995).
21. Baldwin, P.E.J.; Maynard, A.D.: A Survey of Wind Speeds in Indoor Workplaces. Ann Occup Hyg 42(5):303–313 (1996).